

# Change detection needs change information: improving deep 3D point cloud change detection

Iris de Gélis, Thomas Corpetti, Sébastien Lefèvre

**Abstract**—Change detection is an important task that rapidly identifies modified areas, particularly when multi-temporal data are concerned. In landscapes with a complex geometry (e.g., urban environment), vertical information is a very useful source of knowledge that highlights changes and classifies them into different categories. In this study, we focus on change segmentation using raw three-dimensional (3D) point clouds (PCs) directly to avoid any information loss due to the rasterization processes. While deep learning has recently proven its effectiveness for this particular task by encoding the information through Siamese networks, we investigate herein the idea of also using change information in the early steps of deep networks. To do this, we first propose to provide a Siamese KPConv state-of-the-art (SoTA) network with hand-crafted features, especially a change-related one, which improves the mean of the Intersection over Union (IoU) over the classes of change by 4.70%. Considering that a major improvement is obtained due to the change-related feature, we then propose three new architectures to address 3D PC change segmentation: OneConvFusion, Triplet KPConv, and Encoder Fusion SiamKPConv. All these networks consider the change information in the early steps and outperform the SoTA methods. In particular, Encoder Fusion SiamKPConv overtakes the SoTA approaches by more than 5% of the mean of the IoU over the classes of change, emphasizing the value of having the network focus on change information for the change detection task. The code is available at <https://github.com/IdeGelis/torch-points3d-SiamKPConvVariants>.

**Index Terms**—Change detection, deep learning, point clouds

## I. INTRODUCTION

IN an ever-evolving world, being able to sense landscape transformations is of prime importance. The change detection task aims to highlight these modifications from two or more successive observations. Its application in the urban or geoscience domains are numerous, e.g., to easily update maps [1], identify damaged areas in case of natural disasters [2], [3], help city managers [4], [5], highlight coastal modifications [6]–[8], identify glacier melting [9], and detect landslides [10].

Whether for urban [11], [12] or geoscience [13] application, three-dimensional (3D) data, such as Point Clouds (PCs) appear interesting because they provide additional vertical information not available in two-dimensional (2D) images, thereby allowing a better characterization of the complex landscape geometry. In practice, a PC is an unordered and sparse set of

points represented by their 3D coordinates in a frame of reference (e.g., Cartesian coordinate system). For Earth observation purposes, 3D PCs acquired via the photogrammetric process or through Light Detection And Ranging (LiDAR) sensors (e.g., through Aerial Laser Scanning (ALS) for example) are becoming widespread. The specific characteristics of PCs often lead to rasterization into a 2.5D Digital Surface Model (DSM) that can be easily handled using traditional image processing methods [14]–[17]. However, rasterization implies significant information loss, which can be prejudicial; thus, an increasing number of studies is encouraging the design of methods that can deal with raw 3D PCs [18], [19].

We recently [19] showed the possibilities brought by deep learning networks in terms of performing change detection and characterization based on raw PCs. Built upon 2D image change detection deep learning methods [20] and 3D PCs convolutions [21], the Siamese Kernel Point Convolution (KPConv) network outperforms the traditional distance [22], [23], DSM [16], [17] and machine learning-based methods [24] on both real and simulated datasets for multiple change segmentation in urban areas. Aside from this contribution, the literature remains sparse in deep learning methods tackling the change detection at point level, i.e., segmentation of each point of one PC according to the different type of changes compared to the other PC. One can cite the work of [16], [17] that applied deep models to retrieve changes; however, they only focused on 2.5D DSM. By contrast, [25] proposed the processing of a raw 3D PC, thanks to graph convolutions [26]. However, their method was designed for the change classification task, that is, retrieving changes at the scene level, as proposed by the Change3D [25] or Urban 3D Change Detection Classification (Urb3DCD-CIs) [19] datasets. This task is less precise than the change segmentation task because it allows identifying only the main changed object in a scene without precisely localizing it. Hence, the design of new methods that can enhance change segmentation in raw 3D PCs opens up new perspectives.

Considering the limited literature of deep learning methods for 3D PC change detection, all three studies [17], [19], [25] relied on Siamese architecture given its ability to detect changes in 2D remote sensing [20], [27]–[30]. Recent studies on 2D change detection also showed that data fusion is a crucial step in change detection. Therefore, paying more attention on how to fuse information coming from two network inputs and how to incorporate this fused information (i.e., change information) can improve the change detection results. Multi-temporal fusion leads to better results when performed at multiple scales [20], [31]–[33]. While [20] proposed the merging of information from both branches either by feature

Iris de Gélis and Sébastien Lefèvre are with the Institut de Recherche en Informatique et Systèmes Aléatoires (IRISA), UMR 6074, Université Bretagne Sud, Vannes, France (e-mail: iris.de-gelis@irisa.fr, sebastien.lefevre@irisa.fr). Iris de Gélis is also with Magellium, Toulouse, France. Her work is partly funded by the CNES, Toulouse, France. Thomas Corpetti is with the Littoral – Environnement – Télédétection – Géomatique (LETG), UMR 6554, Université Rennes 2, Rennes, France. (e-mail: thomas.corpetti@cnrs.fr).

concatenation or differentiation, others proposed more advanced fusion modules. For example, [34] presented a network based on the three results of feature addition, subtraction, and concatenation at multiple scales. [35] took a step aside from the traditional Siamese network with one input for each branch by proposing to take the image concatenation in one branch and the difference in the other to form two sub-networks with different properties. The features of the two branches were summed at the output of each layer and concatenated at the corresponding scale in the decoder, thanks to skip connections. [36] proposed to embed different fusion modules relying both on the multi-scale feature difference aggregation and attention on the bi-temporal feature concatenation. According to [37], considering both the concatenation and difference of input images is more efficient even in single-stream methods. As with multi-scale, another method category uses attention mechanism to help the network focus on the most important features for the multi-temporal information fusion [34], [38]–[40]. For 3D PC, how to fuse the data from both epochs is not immediately clear because no point-to-point matching exists between the two PCs even in unchanged areas. To deal with this issue, Siamese KPConv includes a nearest-point difference of encoder features at multiple scales. These feature differences are directly integrated into the decoder. Thereby, encoders do not process change information but only mono-date PC without any information on the other PC. We believe that processing change information earlier in the network will boost deep networks toward the final change detection and categorization at point level.

We propose herein the enhancement of the 3D PC change segmentation results based on the consideration that particular attention should be given to change information (i.e., the fusion of information from both dates). We perform the following steps to achieve this enhancement: i) we perform an experiment with additional hand-crafted features, particularly a change-related one, as input along with 3D point coordinates to the existing Siamese KPConv network; ii) we design three new deep learning architectures for the 3D change segmentation; and iii) we prove the effectiveness of the two last items on the public simulated dataset Urban 3D Change Detection (Urb3DCD) [19], [41] as well as on the real dataset Actueel Hoogtebestand Nederland Change Detection (AHN-CD) [19].

The remainder of this paper is structured as follows: Section II describes the hand-crafted features and the three new architectures; Section III provides a method assessment; Section IV discusses the obtained experimental results; and Section V concludes this work.

## II. INCORPORATING CHANGE INFORMATION IN DEEP MODELS

To incorporate the change information in deep networks, we first propose to add some hand-crafted features, also called engineered features, and one change-related feature (Sec. II-A) as input to the current state-of-the-art methods for the 3D PC change detection. We then propose three new deep architectures (Sec. II-B) directly integrating the change information into the encoder and conversely to Siamese KPConv [19].

### A. Considering hand-crafted features

Even if this is not usual in deep learning, some studies showed that combining deep and hand-crafted features improves the final results in computer vision [42] and in remote sensing [43]. [44] showed that incorporating hand-crafted features into a deep learning framework allows the improvement of the PCs semantic segmentation. They evaluated the benefit of giving different feature types in addition to 3D point coordinates for PointNet [45] and PointNet++ [46] 3D deep frameworks. Depending on the dataset (i.e., Mobile Laser Scanning (MLS) or ALS), the PointNet basic architecture can match or even outperform more complex architectures, such as PointNet++ and Kernel Point – Fully Convolutional Neural Network (KP-FCNN) [21], when the input embeds hand-crafted features.

Therefore, we chose to investigate whether or not adding hand-crafted features, particularly a change-related one, in the Siamese KPConv [19] deep network influences the change segmentation results. We used the following hand-crafted features:

- Point distribution represented by their organization in their neighborhood (i.e.,  $L_\lambda$ ,  $P_\lambda$ , and  $O_\lambda$ );
- Point normals ( $N_x$ ,  $N_y$ ,  $N_z$ );
- Height information (i.e.,  $Z_{range}$ ,  $Z_{rank}$ , and  $nH$ );
- Change information (i.e.,  $Stability$ ).

The information on the distribution of points contained in the neighborhood is given by the three following variables: linearity  $L_\lambda$ , planarity  $P_\lambda$ , and omnivariance  $O_\lambda$ . These variables represent the likelihood of a point belonging to a linear (one-dimensional (1D)), a planar (smooth surface) (2D) or a volumetric (3D) neighborhood, respectively. These three attributes are common for extracting information in 3D PCs. They are computed from the three eigenvalues ( $\lambda_1 \geq \lambda_2 \geq \lambda_3 \geq 0$ ) obtained after applying a Principal Component Analysis (PCA) to a matrix containing the 3D coordinates of points in the neighborhood.  $L_\lambda$ ,  $P_\lambda$  and  $O_\lambda$  are given in Equations 1 to 3, respectively.

$$L_\lambda = \frac{\lambda_1 - \lambda_2}{\lambda_1} \quad (1)$$

$$P_\lambda = \frac{\lambda_2 - \lambda_3}{\lambda_1} \quad (2)$$

$$O_\lambda = \sqrt[3]{\lambda_1 \lambda_2 \lambda_3} \quad (3)$$

In practice, if  $\lambda_1$  is larger than  $\lambda_2$  and  $\lambda_3$ ,  $L_\lambda$  is near 1. Only one eigenvalue is meaningful in this case. That is, only one principal axis results from the PCA, and the points are mainly distributed along a single axis. If  $\lambda_1$  and  $\lambda_2$  are larger with regard to  $\lambda_3$ , implying that  $P_\lambda$  is near 1, the points are spread in a plane defined by the eigenvectors corresponding to  $\lambda_1$  and  $\lambda_2$ . Lastly,  $O_\lambda$  is high if each of the three eigenvalues is of equal importance. This implies that the points are scattered along the three axis in a 3D volumetric space.

Once eigenvalues ( $\lambda_1$ ,  $\lambda_2$ ,  $\lambda_3$ ) are computed, point normals ( $N_x$ ,  $N_y$ ,  $N_z$ ) are obtained by taking the eigenvector corresponding to the smallest eigenvalue.

$Z_{range}$  and  $Z_{rank}$  provide the height information by providing the maximum height (Z coordinate) difference between the

points in the neighborhood and the rank of the height of the considered points within the neighborhood. The normalized height  $nH$  completes the height information by providing the difference between the height of the considered points and the local Digital Terrain Model (DTM) (rasterization of the PC at the ground level).

Lastly, the *Stability* [24] feature provides a bi-temporal information on the considered point. It is the ratio of the number of points in the spherical neighborhood to the number of points in the vertical cylindrical neighborhood in the other PC (oriented along the vertical axis). Thus, in each point of the current PC, *Stability* is the ratio between the number of points in the 3D ( $n_{3D}$ ) and 2D ( $n_{2D}$ ) neighborhoods in the other PC, in present :

$$Stability = \frac{n_{3D}}{n_{2D}} \times 100 \quad (4)$$

Looking only at the number of points in the 3D neighborhood of each point of both PCs is enough to retrieve the changes on isolated buildings and trees. However, in dense forest areas or when different objects are close to each other, the 3D spherical neighborhood may still contain points coming from some other unchanged entity. Hence, taking the ratio with the 2D neighborhood is a way to consider the unchanged points and obtain an indicator of change and object instability. The ratio will be near 100% if no change occurs and tends to 0% in case of changes. We expect the *Stability* value of vegetation to be lower. Most of the hand-crafted features presented in [24] are used except for those that utilize LiDAR's multi-target capability, because our datasets do not contain such information (see Section III-A). We recall that the Siamese KPConv architecture takes as many input features as desired, by simply modifying the number of inputs of the first layer of encoders.

### B. New models for 3D point cloud change detection

We will now explore how to learn this change information through novel deep networks. We built upon the Siamese KPConv model to propose three original architectures emphasizing the change-related features. The three presented architectures are based on Kernel Point Convolution (KPConv) [21] because it had been proven efficient for the change detection task in 3D PCs. We fused the features coming from both PCs by using the nearest-point difference strategy, as in Siamese KPConv:

$$(\mathcal{P}_1, \mathcal{F}_1) \ominus (\mathcal{P}_2, \mathcal{F}_2) = f_{2i} - f_{1j | j = \arg \min (\|x_{2i} - x_{1j}\|)} \quad (5)$$

Thus, for PCs  $\mathcal{P}_1$  and  $\mathcal{P}_2$ , with their corresponding features  $\mathcal{F}_1$  and  $\mathcal{F}_2$ , the feature difference  $\ominus$  was computed between features  $f_{2i} \in \mathcal{F}_2$  of each point  $x_{2i} \in \mathcal{P}_2$  of the second PC and features  $f_{1j} \in \mathcal{F}_1$  of the nearest-point  $x_{1j} \in \mathcal{P}_1$ .

The first option was to create a relatively simple network by fusing the information of both PCs just after the first layer (Figure 1). The following layer of the encoder took as input only the nearest-point feature difference (noted  $\ominus$ ). The following layers of the encoder and the decoder took as input the output of the previous layer, as in a classical Fully Convolutional Network (FCN). Here, the idea was to evaluate

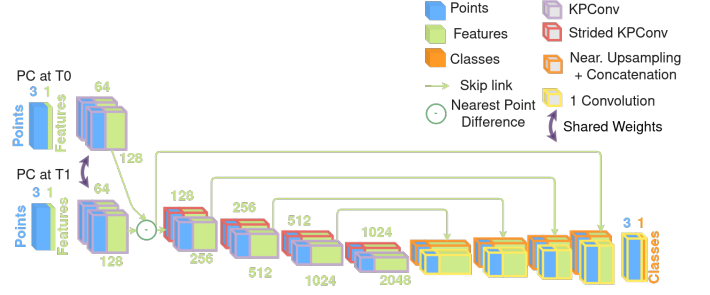


Fig. 1. OneConvFusion architecture for the 3D PC change segmentation. The links between successive layers were omitted for brevity.

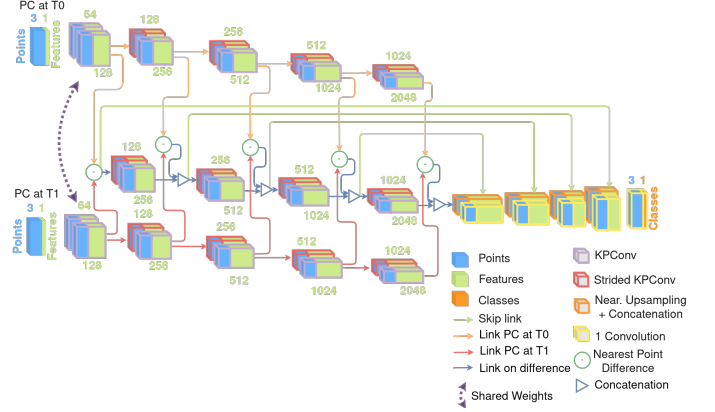


Fig. 2. Triplet KPConv architecture for 3D the PCs change segmentation.

the benefits of dealing with differences early in the process. This architecture is called OneConvFusion.

However, the mono-date features of the first layer might not be sufficient for accurate change identification. Therefore, we designed the Triplet KPConv network (Figure 2), that contained two encoders for extracting the mono-date information (as in the Siamese KPConv network) and an additional encoder that extracts the change-related features. The “change encoder” took as input the nearest-point difference computed after the first layer of the mono-date encoders. The following layers of the change encoder took as input the output feature concatenation of the previous layer and the result of the nearest-point features (from the mono-date encoder) difference of the corresponding scale. The multi-scale mono-date and change information were both considered. The decoder used the features extracted by the change encoder as the input. Note that mono-date encoders can either share weights or not, the latter leading to the Pseudo-Triplet KPConv, as for Siamese KPConv, and a Pseudo-Siamese KPConv. Therefore, in a shared-weight configuration, the Triplet KPConv network is as symmetrical as the Siamese KPConv.

The third version of the architecture was designed to directly fuse the mono-date and change features in the same encoder. This network is called Encoder Fusion SiamKPConv. The first encoder extracted the mono-date features of the older PC using convolution layers (top, Figure 3), as in all previous architectures. As illustrated in the bottom of Figure 3, the second encoder more specifically combined the output features from the newer PC and the nearest point feature difference.

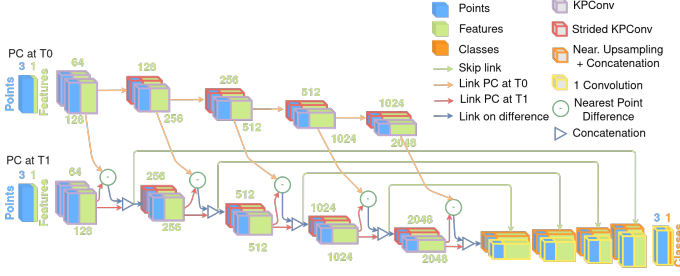


Fig. 3. Encoder Fusion SiamKPCConv architecture for the 3D PC change segmentation.

Each layer of this second encoder took as input the output feature concatenation of the previous layer and the difference of the features from this encoder and the mono-date encoder of the older PC. Hence, both mono-date and change features can be combined in convolutional layers. Note that this third architecture is not symmetrical, in contrast to the previous ones, because the weights of the two encoders were obviously not shared. As regards the Triplet KPCConv and OneConvFusion architectures, the idea was to encode the differences earlier in the process. In this third architecture, however, we fused them with the features of the second PC to better combine the two different feature types.

These proposed new architectures are in line with the recent developments for the 2D image change detection in terms of the importance of data fusion [31], [35], [36] for the change detection task. By convolving the change features in the encoder, we expect the network to put more attention on the changes and better combine the multi-scale change features.

### III. RESULTS

The experimental results of our methods are elaborated here on public simulated and real datasets to quantitatively evaluate our networks. Before we describe them in detail, let us first introduce the experimental settings.

#### A. Datasets

The public dataset Urban 3D Change Detection (Urb3DCD) [41] was used for our experiments. This dataset comprised various semantic change situations inside cities based on real information related to the organization of streets, areas, etc., on which buildings, vegetation, or cars have been added. It then simulates point clouds derived from laser pulses from ALS with real flight plans.

Among the different dataset versions, we chose to assess the one with a low point density (approximately 0.5 points/m<sup>2</sup>) because it contains more change classes (i.e., ‘unchanged’, ‘new building’, ‘demolition’, ‘new vegetation’, ‘vegetation growth’, ‘missing vegetation’ and ‘mobile object’) and it relies on PCs that are more realistic than the first dataset version [19].

Some quantitative results are given using the Actueel Hoogtebestand Nederland Change Detection (AHN-CD) dataset presented in [19] to prove the effectiveness of our

methods on real data. This dataset is composed of two dates of the ALS surveys over the Netherlands. The PC densities varied from 10 to 14 points/m<sup>2</sup> for the first date (AHN3) and 10 to 24 points/m<sup>2</sup> for the second date (AHN4). Some change annotations were semi-automatically derived from the mono-date semantic labeling for the training and validation sets. The test set was manually annotated to avoid any labeling errors present in the semi-automatic annotation. In addition to the ‘unchanged’ classes, this dataset also contains the three following change classes: ‘new building’, ‘demolition’, and ‘new clutter’.

#### B. Experimental settings

For the experimental settings, we utilized the hyperparameters used by [19] for Siamese KPCConv. Some cylinder pairs of 50 m radius were extracted from both the PCs for Urb3DCD. The first sub-sampling rate  $dl_0$  was set to 1 m. A radius of 25 m was used for the AHN-CD dataset with a first sub-sampling rate  $dl_0$  set to 0.5 m. For training purposes, we minimized the negative log-likelihood (NLL) loss using a Stochastic Gradient Descent (SGD) with a 0.98 momentum. The loss was calculated as follows:

$$NLL(y_t, y_p) = -(y_t \log(y_p) + (1 - y_t) \log(1 - y_p)) \quad (6)$$

where  $y_t$  corresponds to the target label’s probability and  $y_p$  is the predicted label’s probability. Ten cylinder pairs were used in each batch. The initial learning rate was set to  $10^{-2}$  and scheduled to decrease exponentially. For the training we relied on a random drawing of training cylinders as a function of the class distribution as in [19], because the change detection dataset was generally imbalanced. For each training epoch, 6,000 cylinder training pairs were seen by the network. A total of 3,000 pairs from the validation set were used during the validation. The loss was weighted according to the class distribution to ensure learning the less-represented classes as well. Data augmentation was performed during training through the random rotation of cylinders around the vertical axis (note: both cylinders of a pair were rotated by the same angle to keep the coherence inside the pair) and the addition of a Gaussian noise at point level.

The development of these architectures was implemented in PyTorch and relied on the KPCConv implementation available in Torch-Points3D [47]. For the nearest-point feature difference (Equation 5), the nearest point was determined by the k-Nearest Neighbors (kNN) implementation available in the graphics processing unit (GPU)-compliant PyTorch Geometric for a faster computation.

For the hand-crafted feature extraction, the computation is made before the cylinder extraction to limit border effects. Neighborhood sizes for the *Stability* are set at 5 m for Urb3DCD and 3 m for AHN-CD. Concerning other neighborhoods, they are based on the 10 nearest neighbor points. Point normal and DTM computations are performed using Point Data Abstraction Library (PDAL)<sup>1</sup>.

In change detection and categorization, datasets are largely imbalanced. In other words, most of the data belong to the

<sup>1</sup><https://pdal.io/en/2.5-maintenance/index.html>, accessed on 27/02/2023.

TABLE I  
COMPARISON OF SIAMESE KPConv NETWORK WITH DIFFERENT INPUT FEATURES ON THE URB3DCD-V2 LOW-DENSITY LiDAR DATASET. THE RESULTS ARE GIVEN IN %. THE 10 INPUT FEATURES ARE AS FOLLOWS:  $N_x$ ,  $N_y$ ,  $N_z$ ,  $L_T$ ,  $P_T$ ,  $O_T$ ,  $Z_{range}$ ,  $Z_{rank}$ ,  $nH$  AND *Stability*.

# of input features	mAcc	mIoU <sub>ch</sub>
0	91.21 ± 0.68	80.12 ± 0.02
10	<b>93.65</b> ± 0.16	<b>84.82</b> ± 0.58
9 w/o <i>Stability</i>	91.44 ± 0.47	80.49 ± 0.64
1 <i>Stability</i> only	92.92 ± 0.47	83.80 ± 0.89

unchanged class, despite this class not being the most interesting one. Hence, we preferred herein to disregard the overall accuracy or precision scores that were not very indicative of the method's performance under these settings. Accordingly, we selected the mean accuracy (mAcc) and the mean of the Intersection over Union (IoU) over the classes of change (mIoU<sub>ch</sub>) for a more reliable quantitative assessment of the different methods.

All tests were conducted three times to assess the variability in the results. The average results of these three runs are given along with the standard deviation in Tables I, II, III and IV.

### C. Experimental results

1) *Results of adding hand-crafted features to the Siamese KPConv network:* Table I presents the quantitative results. Note that the results given with zero input features corresponded to those reported in the original publication of the Siamese KPConv [19]. Providing the hand-crafted features as input in addition to the point coordinates considerably improved the results. We subsequently assessed the importance of the unique change-related hand-crafted feature, the *Stability*. The point distribution and the height hand-crafted features seem to have only a slight beneficial impact (+0.37% of mIoU<sub>ch</sub>) on the change segmentation results. In contrast, the *Stability* feature seems to have a major impact (+3.67% of mIoU<sub>ch</sub>) on both metrics mAcc and mIoU<sub>ch</sub>. More specifically, when looking at the per class gain in the IoU, the *Stability* feature on its own principally helped in the 'new building', 'demolition' and 'missing vegetation' classes (Figure 4).

2) *Results of the Siamese KPConv evolution:* Tables II and III present the quantitative results of the evaluation of the three architectures on the Urb3DCD-V2 dataset. Each of the three architectures outperformed the Siamese KPConv network. The best architecture was Encoder Fusion SiamKPConv, followed by Triplet KPConv. OneConvFusion performed only slightly better with a 1.5% of the mIoU<sub>ch</sub> when compared with Siamese KPConv. Looking at the per-class results (Table III and Figure 5), the Encoder Fusion SiamKPConv network provided a significant improvement for all change classes. Figures 6 and 7 depict the qualitative results. The three architectures provided very similar results to the ground truth. In Figure 7, each of the three Siamese KPConv evolutions showed results that were more accurate than those in Siamese KPConv in the new building facades. These facades were particularly hard to correctly detect because the neighboring

TABLE II  
RESULTS IN % OF THE THREE SIAMESE KPConv EVOLUTIONS ON THE URB3DCD-V2 LOW DENSITY LiDAR DATASET.

Method	mAcc (%)	mIoU <sub>ch</sub> (%)
Siamese KPConv [19]	91.21 ± 0.68	80.12 ± 0.02
Siamese KPConv (+10 input features)	93.65 ± 0.16	84.82 ± 0.58
OneConvFusion	92.62 ± 1.10	81.74 ± 1.45
Triplet KPConv	92.94 ± 0.53	84.08 ± 1.20
Encoder Fusion SiamKPConv	<b>94.23</b> ± 0.88	<b>85.19</b> ± 0.24

facade was not visible in the first PC (Figure 7a). Therefore, identifying the new facade in the class 'new building' while the neighboring facades were unchanged was not obvious. In this situation, the network should understand that the facade may be new because the roof is new. In the same manner, a roof that remains unchanged should also have an unchanged facade. Another difference with the Siamese KPConv results can be found in Figure 6 (zoomed out portions), where a part of the church roof is identified as new vegetation for Siamese KPConv only, not for the other architectures. The misclassification was probably due to the dome roof shape that looked like a tree in the simulated data. Even if the tree models were not totally spherical (i.e., the Arbraro software [48] was used to obtain OBJ models of trees, see [19]), the LiDAR simulation on these models rendered a quite spherical object with only a few points inside the foliage of the tree, unlike the real LiDAR acquisition. Therefore, aside from the shape, the main factor for distinguishing between vegetation and the dome is that trees are generally on the ground. These examples highlight the fact that the network should be able to understand the PC at multiple scales and predict changes with regard to the surrounding objects.

Table IV presents the quantitative results for the experiments on the real data. All proposed architectures and exploitation of the hand-crafted features enabled us to improve the state-of-the-art Siamese KPConv results. Encoder Fusion SiamKPConv and OneConvFusion showed the largest improvements of up to approximately 5% of the mIoU<sub>ch</sub>. In contrast to the results on the Urb3DCD-V2 results, OneConvFusion obtained results comparable with those of Encoder Fusion SiamKPConv, albeit with a larger standard deviation. Given that the training set for AHN-CD included numerous labeling errors and considering the standard deviations of OneConvFusion and Encoder Fusion SiamKPConv, these two approaches were similar in terms of performance. Although OneConvFusion achieved only a minor enhancement in Urb3DCD-V2, it produced results that yielded a significant improvement on the AHN-CD dataset similar to Encoder Fusion SiamKPConv. OneConvFusion is a network with fewer parameters compared to other methods (Table V). This probably led to a better generalization of the training data and ended up in superior results despite the numerous errors present in the training database.

## IV. DISCUSSION

### Number of parameters

While it was important to study the predicted change detection results, it is also relevant to check the number of trainable parameters in each architecture. Table V shows that

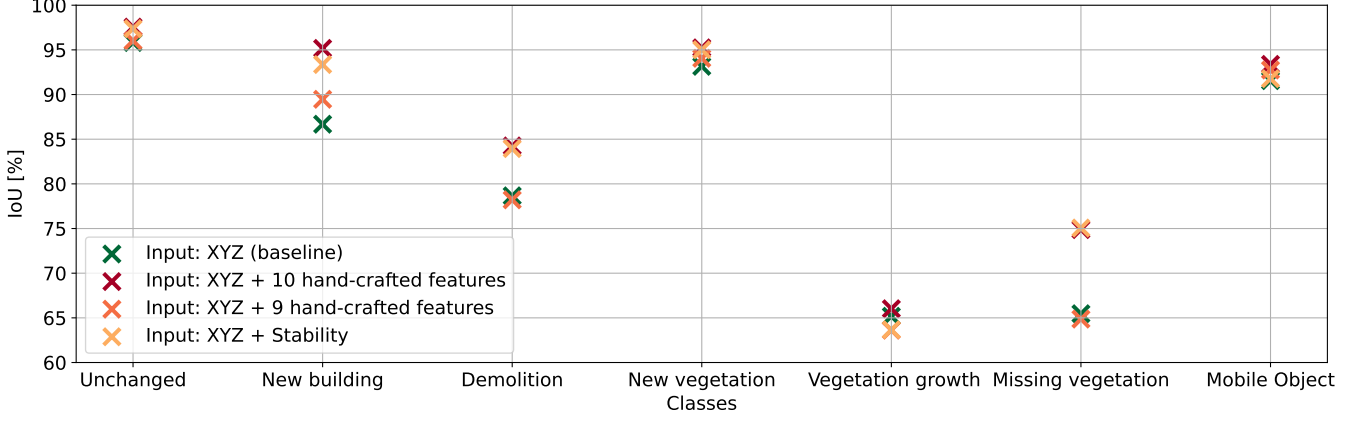


Fig. 4. **Influence on per class IoU of adding hand-crafted features along with 3D point coordinates as the input to the Siamese KPConv.** For the ‘new building’, ‘demolition’ and ‘missing vegetation’ classes, the high disparity in the IoU demonstrated that adding the hand-crafted features as input had a larger influence compared to those on classes where the results were grouped around the same value.

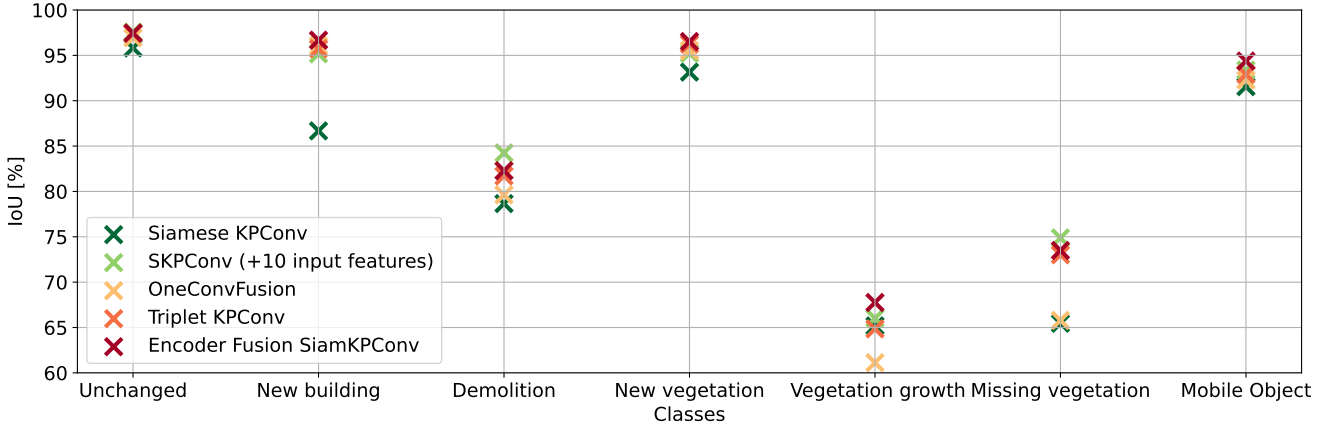


Fig. 5. **Influence on per class IoU of the three Siamese KPConv evolutions**, namely OneConvFusion, Triplet KPConv and Encoder Fusion SiamKPConv. The results of Siamese KPConv with 10 hand-crafted input features were also included for comparison purposes.

Triplet KPConv and Encoder Fusion SiamKPConv required approximately two times more trainable parameters, whereas OneConvFusion needed exactly the same number of parameters as Siamese KPConv. Adding input features only slightly increased the number of parameters. This must be considered in case of limited training capabilities. Directly guiding the network to change detection by introducing hand-crafted features seems interesting in preventing a drastic increase of trainable parameters.

#### Importance of learning change information

An immediate observation from our experiments was that adding hand-crafted features related to both input data as the input to the Siamese KPConv network did not bring any significant change on the results (Table II, third line –Addition of features– compared to the first one).

Looking at the results presented in [19], the Siamese KPConv architecture was able to detect the change on its own; however, it seems that giving a hand-crafted feature related to

the change specifically as an input helps the network focus on the change with a significant improvement (Table II, fourth line –Addition of a change feature– compared to the first one).

This finding underlines the fact that encoding change information is important. On this basis, we confirm that the proposed evolutions of Siamese KPConv depict the relevance of applying convolution on the nearest-point feature difference at multiple scales to obtain change-related features (Table III three last lines) not by introducing change features, but by encoding them directly. The somewhat worse results of the OneConvFusion network, specifically on Urb3DCD, exhibit the importance of keeping multi-scale mono-date features in the architecture. Note that this is in line with the deep learning for the change detection literature in 2D [20], [31]–[33]. The fact that Encoder Fusion SiamKPConv provided better results compared to the Triplet network showed that combining both mono-date semantic and change features as input to the convolutional layers enables the extraction of useful discriminative features for the change segmentation task. Note that both Triplet KPConv and Encoder Fusion SiamKPConv obtained



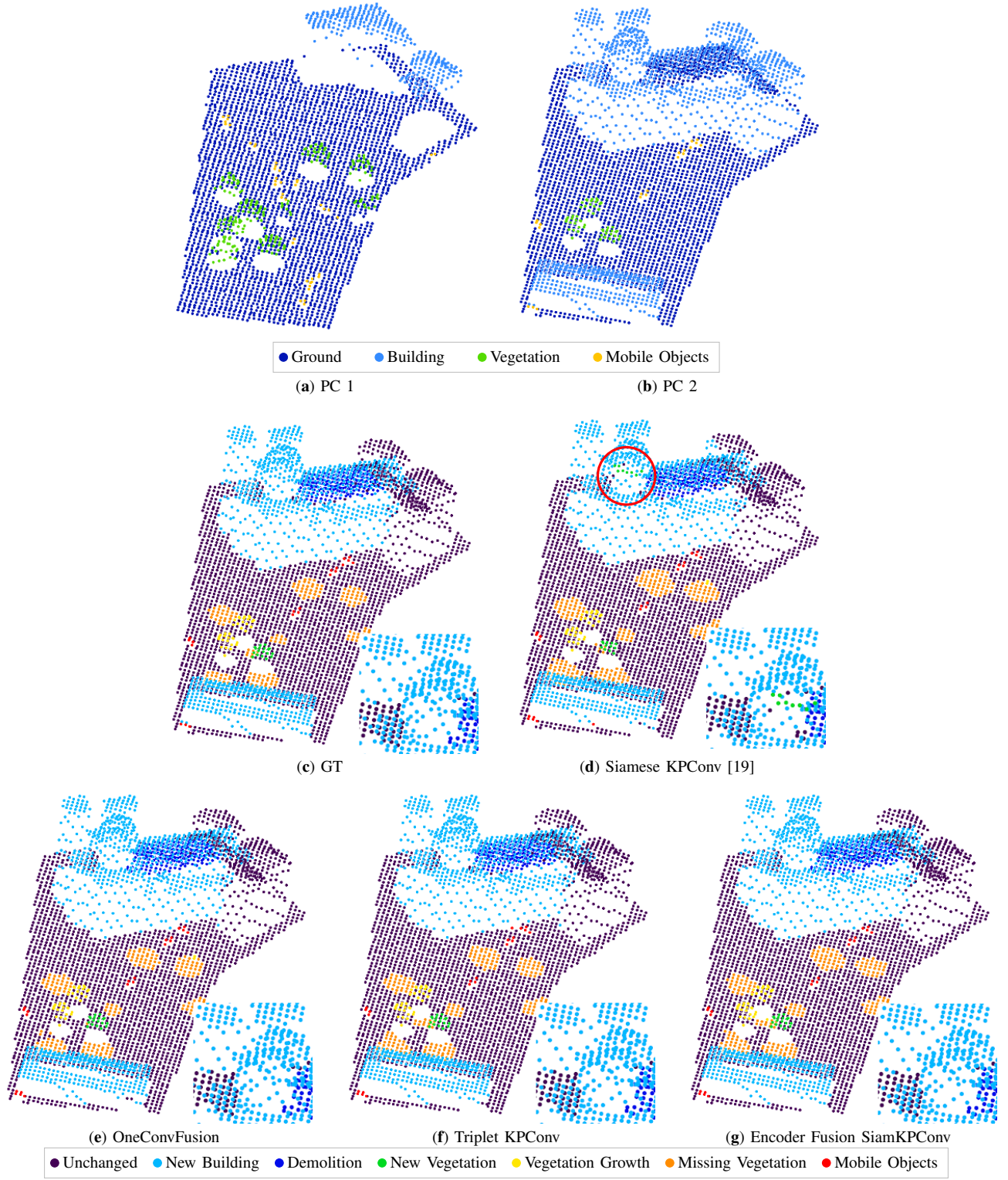


Fig. 6. **Visual change detection results on the Urb3DCD-V2 low-density LiDAR sub-dataset:** (a-b) two input point clouds; (c) ground truth (GT): simulated changes; (d) Siamese KPConv results; (e) OneConvFusion results; (f) Triplet KPConv results; and (g) Encoder Fusion SiamKPConv results. The region of interest specifically discussed in the text was highlighted with an ellipse.

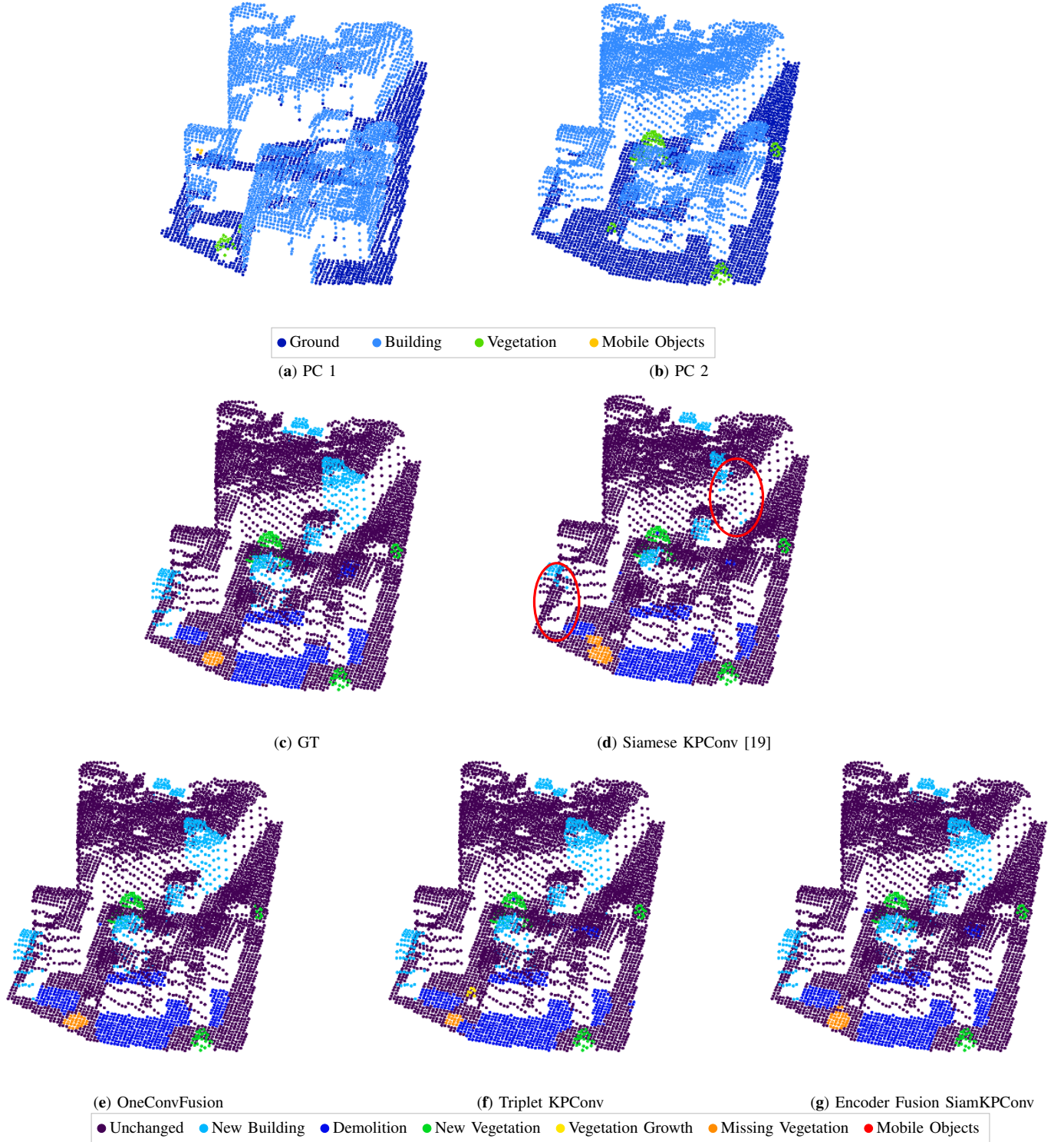


Fig. 7. **Visual change detection results on the Urb3DCD-V2 low density LiDAR sub-dataset in an area containing occlusions:** (a-b) two input point clouds; (c) ground truth (GT): simulated changes; (d) Siamese KPConv results; (e) OneConvFusion results; (f) Triplet KPConv results; and (g) Encoder Fusion SiamKPConv results. The regions of interest specifically discussed in the text were highlighted with ellipses.



TABLE III  
PER-CLASS IOU SCORES OF THE THREE SIAMESE KPConv EVOLUTIONS ON THE URB3DCD-V2 LOW DENSITY LiDAR DATASET. THE RESULTS WERE GIVEN IN %. VEG.: VEGETATION; INPUT FEAT.: INPUT FEATURES; AND SKPConv: SIAMESE KPConv.

Method	Per class IoU (%)						
	Unchanged	New building	Demolition	New veg.	Veg. growth	Missing veg.	Mobile Object
Siamese KPConv [19]	95.82 ± 0.48	86.67 ± 0.47	78.66 ± 0.47	93.16 ± 0.27	65.18 ± 1.37	65.46 ± 0.93	91.55 ± 0.60
SKPConv (+10 input feat.)	<b>97.55</b> ± 0.11	95.17 ± 0.21	<b>84.25</b> ± 0.59	95.23 ± 0.21	66.02 ± 1.33	<b>74.88</b> ± 1.03	93.38 ± 0.74
OneConvFusion	96.95 ± 0.34	96.06 ± 0.27	79.63 ± 1.48	95.53 ± 0.77	61.12 ± 2.13	65.79 ± 2.61	92.89 ± 1.95
Triplet KPConv	97.41 ± 0.24	95.73 ± 0.67	81.71 ± 1.47	96.24 ± 0.37	64.85 ± 1.46	73.02 ± 1.18	92.90 ± 2.47
Encoder Fusion SKPConv	97.47 ± 0.04	<b>96.68</b> ± 0.30	82.29 ± 0.16	<b>96.52</b> ± 0.03	<b>67.76</b> ± 1.51	73.50 ± 0.81	<b>94.37</b> ± 0.54

TABLE IV  
RESULTS IN % OF THE THREE SIAMESE KPConv EVOLUTIONS ON THE MANUALLY CLEANED AHN-CD DATASET.

Method	mAcc (%)	mIoU <sub>ch</sub> (%)
Siamese KPConv [19]	85.65 ± 1.55	70.65 ± 2.05
Siamese KPConv (+10 input features)	88.47 ± 1.09	73.29 ± 1.32
OneConvFusion	90.03 ± 0.38	<b>75.62</b> ± 1.04
Triplet KPConv	88.25 ± 0.23	72.37 ± 0.55
Encoder Fusion SiamKPConv	<b>90.26</b> ± 0.22	75.00 ± 0.74

TABLE V  
NUMBER OF PARAMETERS IN EACH PRESENTED ARCHITECTURE COMPARED TO THOSE OF THE ORIGINAL SIAMESE KPConv NETWORK.

Method	Number of parameters
Siamese KPConv [19]	18,441,152
Siamese KPConv (+10 input features)	18,457,152
OneConvFusion	18,441,152
Triplet KPConv	39,753,536
Encoder Fusion SiamKPConv	39,841,152

results close to (or even outperformed) the Siamese KPConv network with the 10 hand-crafted features.

Finally, we added hand-crafted features as the Encoder Fusion SiamKPConv network input. The results were only very slightly improved at less than 1% of the mIoU<sub>ch</sub>. In other words, an architecture more specifically designed for change detection can extract discriminative features on its own. This is especially true for the change-related feature of *Stability*, which is no longer required in the Encoder Fusion SiamKPConv architecture.

## V. CONCLUSION

In this work, we proposed the enhancement of change detection in raw 3D PCs by using deep networks. We suggested the introduction of the change information early in the network to better detect and categorize the changes in 3D PCs. The first proposition for enhancing the existing method was to provide some hand-crafted features as input along with 3D point coordinates. We demonstrated that the addition of a single change-related feature input to the existing Siamese KPConv method yields an enhancement of approximately 3.70% of the mean of the IoU over change classes. We also proposed three new architectures for change segmentation based on raw 3D PCs that encoded the change information conversely to the current state-of-the-art, which only incorporated change information in the decoder step. All three architectures outperformed the current SOTA methods by up to 5.07% of the mean of the IoU over classes of change. In conclusion, the

importance of encoding change information was confirmed in this investigation.

As for future work, we mainly see two axes of improvement. First one could imagine introducing attention mechanism for multi-scale fusion of both change-related and mono-date features, as was already successfully shown in recent studies in 2D image change detection [36], [40], [49]. Investigating transformers [50] is an interesting perspective for the improvement of our method. However, their scaling to large remote sensing PCs is often not obvious. Finally, these architectures need to be trained on large amounts of data to obtain convincing results. Considering the difficulty of PC annotation, the second axis of improvement is to focus on semi-supervised methods for the 3D change detection.

## ACKNOWLEDGMENT

This research was funded by Magellium and the CNES, Toulouse, with access to the HPC resources of IDRIS under the allocation 2022-AD011011754R2 made by GENCI.

## REFERENCES

- [1] N. Champion, D. Boldo, M. Pierrot-Deseilligny, and G. Stamon, "2d building change detection from high resolution satellite imagery: A two-step hierarchical method based on 3d invariant primitives," *Pattern Recognition Letters*, vol. 31, no. 10, pp. 1138–1147, 2010.
- [2] J. Sublime and E. Kalinicheva, "Automatic post-disaster damage mapping using deep-learning techniques for change detection: Case study of the tohoku tsunami," *Remote Sensing*, vol. 11, no. 9, p. 1123, 2019.
- [3] V. Zahs, K. Anders, J. Kohns, A. Stark, and B. Höfle, "Classification of structural building damage grades from multi-temporal photogrammetric point clouds using a machine learning model trained on virtual laser scanning data," *arXiv preprint arXiv:2302.12591*, 2023.
- [4] I. Sandric, B. Mihai, I. Savulescu, B. Suditu, and Z. Chitu, "Change detection analysis for urban development in bucharest-romania, using high resolution satellite imagery," in *2007 Urban Remote Sensing Joint Event*. IEEE, 2007, pp. 1–8.
- [5] J. Feranec, G. Hazeu, S. Christensen, and G. Jaffrain, "Corine land cover change detection in europe (case studies of the netherlands and slovakia)," *Land use policy*, vol. 24, no. 1, pp. 234–247, 2007.
- [6] P. Letortu, S. Costa, O. Maquaire, C. Delacourt, E. Augereau, R. Davidson, S. Suanez, and J. Nabucet, "Retreat rates, modalities and agents responsible for erosion along the coastal chalk cliffs of Upper Normandy: The contribution of terrestrial laser scanning," *Geomorphology*, vol. 245, pp. 3–14, Sep. 2015.
- [7] A. R. Enríquez, M. Marcos, A. Falqués, and D. Roelvink, "Assessing beach and dune erosion and vulnerability under sea level rise: a case study in the mediterranean sea," *Frontiers in Marine Science*, vol. 6, p. 4, 2019.
- [8] I. de Gélis, Z. Bessin, P. Letortu, M. Jaud, C. Delacourt, S. Costa, O. Maquaire, R. Davidson, T. Corpetti, and S. Lefèvre, "Cliff change detection using siamese kpconv deep network on 3d point clouds," *ISPRS Annals of the Photogrammetry, Remote Sensing and Spatial Information Sciences*, vol. V-3-2022, pp. 649–656, 2022.
- [9] R. Hock, "Glacier melt: a review of processes and their modelling," *Progress in physical geography*, vol. 29, no. 3, pp. 362–391, 2005.

- [10] B. D. Malamud, D. L. Turcotte, F. Guzzetti, and P. Reichenbach, "Landslide inventories and their statistical properties," *Earth Surface Processes and Landforms*, vol. 29, no. 6, pp. 687–711, 2004.
- [11] U. Stilla and Y. Xu, "Change detection of urban objects using 3d point clouds: A review," *ISPRS Journal of Photogrammetry and Remote Sensing*, vol. 197, pp. 228–255, 2023.
- [12] W. Xiao, H. Cao, M. Tang, Z. Zhang, and N. Chen, "3d urban object change detection from aerial and terrestrial point clouds: A review," *International Journal of Applied Earth Observation and Geoinformation*, vol. 118, p. 103258, 2023.
- [13] R. Qin, J. Tian, and P. Reinartz, "3D change detection – approaches and applications," *ISPRS Journal of Photogrammetry and Remote Sensing*, vol. 122, pp. 41–56, 2016.
- [14] H. Murakami, K. Nakagawa, H. Hasegawa, T. Shibata, and E. Iwanami, "Change detection of buildings using an airborne laser scanner," *ISPRS Journal of Photogrammetry and Remote Sensing*, vol. 54, no. 2-3, pp. 148–152, 1999.
- [15] C. Stal, F. Tack, P. De Maeyer, A. De Wulf, and R. Goossens, "Airborne photogrammetry and lidar for dsm extraction and 3d change detection over an urban area—a comparative study," *International Journal of Remote Sensing*, vol. 34, no. 4, pp. 1087–1110, 2013.
- [16] Z. Zhang, G. Vosselman, M. Gerke, D. Tuia, and M. Y. Yang, "Change detection between multimodal remote sensing data using siamese cnn," *arXiv preprint arXiv:1807.09562*, 2018.
- [17] Z. Zhang, G. Vosselman, M. Gerke, C. Persello, D. Tuia, and M. Yang, "Detecting building changes between airborne laser scanning and photogrammetric data," *Remote sensing*, vol. 11, no. 20, p. 2417, 2019.
- [18] T. G. Bernard, D. Lague, and P. Steer, "Beyond 2d landslide inventories and their rollover: synoptic 3d inventories and volume from repeat lidar data," *Earth Surface Dynamics*, vol. 9, no. 4, pp. 1013–1044, 2021.
- [19] I. de Gélis, S. Lefèvre, and T. Corpetti, "Siamese kpconv: 3d multiple change detection from raw point clouds using deep learning," *ISPRS Journal of Photogrammetry and Remote Sensing*, vol. 197, pp. 274–291, 2023.
- [20] R. C. Daudt, B. Le Saux, and A. Boulch, "Fully convolutional siamese networks for change detection," in *2018 25th IEEE International Conference on Image Processing (ICIP)*. IEEE, 2018, pp. 4063–4067.
- [21] H. Thomas, C. R. Qi, J.-E. Deschaud, B. Marcotegui, F. Goulette, and L. J. Guibas, "Kpconv: Flexible and deformable convolution for point clouds," in *Proceedings of the IEEE/CVF International Conference on Computer Vision*, 2019, pp. 6411–6420.
- [22] D. Girardeau-Montaut, M. Roux, R. Marc, and G. Thibault, "Change detection on points cloud data acquired with a ground laser scanner," *International Archives of Photogrammetry, Remote Sensing and Spatial Information Sciences*, vol. 36, no. part 3, p. W19, 2005.
- [23] D. Lague, N. Brodu, and J. Leroux, "Accurate 3D comparison of complex topography with terrestrial laser scanner: Application to the rangitikei canyon (NZ)," *ISPRS Journal of Photogrammetry and Remote Sensing*, vol. 82, pp. 10–26, 2013.
- [24] T. Tran, C. Ressel, and N. Pfeifer, "Integrated change detection and classification in urban areas based on airborne laser scanning point clouds," *Sensors*, vol. 18, no. 2, p. 448, 2018.
- [25] T. Ku, S. Galanakis, B. Boom, R. C. Velkamp, D. Bangera, S. Gangisetty, N. Stagakis, G. Arvanitis, and K. Moustakas, "Shrec 2021: 3d point cloud change detection for street scenes," *Computers & Graphics*, vol. 99, pp. 192–200, 2021.
- [26] Y. Wang, Y. Sun, Z. Liu, S. E. Sarma, M. M. Bronstein, and J. M. Solomon, "Dynamic graph cnn for learning on point clouds," *ACM Transactions On Graphics (TOG)*, vol. 38, no. 5, pp. 1–12, 2019.
- [27] Y. Zhan, K. Fu, M. Yan, X. Sun, H. Wang, and X. Qiu, "Change detection based on deep siamese convolutional network for optical aerial images," *IEEE Geoscience and Remote Sensing Letters*, vol. 14, no. 10, pp. 1845–1849, 2017.
- [28] S. Lefèvre, D. Tuia, J. D. Wegner, T. Produit, and A. S. Nassar, "Toward seamless multiview scene analysis from satellite to street level," *Proceedings of the IEEE*, vol. 105, no. 10, pp. 1884–1899, 2017.
- [29] H. He, M. Chen, T. Chen, and D. Li, "Matching of remote sensing images with complex background variations via siamese convolutional neural network," *Remote Sensing*, vol. 10, no. 2, p. 355, 2018.
- [30] W. Shi, M. Zhang, R. Zhang, S. Chen, and Z. Zhan, "Change detection based on artificial intelligence: State-of-the-art and challenges," *Remote Sensing*, vol. 12, no. 10, p. 1688, 2020.
- [31] H. Chen, C. Wu, B. Du, and L. Zhang, "Deep siamese multi-scale convolutional network for change detection in multi-temporal vhr images," in *2019 10th International Workshop on the Analysis of Multitemporal Remote Sensing Images (MultiTemp)*. IEEE, 2019, pp. 1–4.
- [32] M. Zhang and W. Shi, "A feature difference convolutional neural network-based change detection method," *IEEE Transactions on Geoscience and Remote Sensing*, vol. 58, no. 10, pp. 7232–7246, 2020.
- [33] X. Zheng, D. Guan, B. Li, Z. Chen, and L. Pan, "Global and local graph-based difference image enhancement for change detection," *Remote Sensing*, vol. 15, no. 5, p. 1194, 2023.
- [34] L. Song, M. Xia, J. Jin, M. Qian, and Y. Zhang, "Suacnet: Attentional change detection network based on siamese u-shaped structure," *International Journal of Applied Earth Observation and Geoinformation*, vol. 105, p. 102597, 2021.
- [35] K. Jiang, W. Zhang, J. Liu, F. Liu, and L. Xiao, "Joint variation learning of fusion and difference features for change detection in remote sensing images," *IEEE Transactions on Geoscience and Remote Sensing*, vol. 60, pp. 1–18, 2022.
- [36] H. Yin, L. Weng, Y. Li, M. Xia, K. Hu, H. Lin, and M. Qian, "Attention-guided siamese networks for change detection in high resolution remote sensing images," *International Journal of Applied Earth Observation and Geoinformation*, vol. 117, p. 103206, 2023. [Online]. Available: <https://www.sciencedirect.com/science/article/pii/S1569843223000286>
- [37] X. Peng, R. Zhong, Z. Li, and Q. Li, "Optical remote sensing image change detection based on attention mechanism and image difference," *IEEE Transactions on Geoscience and Remote Sensing*, vol. 59, no. 9, pp. 7296–7307, 2020.
- [38] H. Jiang, X. Hu, K. Li, J. Zhang, J. Gong, and M. Zhang, "Pga-siamnet: Pyramid feature-based attention-guided siamese network for remote sensing orthoimagery building change detection," *Remote Sensing*, vol. 12, no. 3, p. 484, 2020.
- [39] P. Chen, L. Guo, X. Zhang, K. Qin, W. Ma, and L. Jiao, "Attention-guided siamese fusion network for change detection of remote sensing images," *Remote Sensing*, vol. 13, no. 22, p. 4597, 2021.
- [40] J. Chen, J. Fan, M. Zhang, Y. Zhou, and C. Shen, "Msf-net: A multiscale supervised fusion network for building change detection in high-resolution remote sensing images," *IEEE Access*, vol. 10, pp. 30 925–30 938, 2022.
- [41] I. de Gélis, S. Lefèvre, and T. Corpetti, "Change detection in urban point clouds: An experimental comparison with simulated 3d datasets," *Remote Sensing*, vol. 13, no. 13, 2021.
- [42] L. Nanni, S. Ghidoni, and S. Brahmam, "Handcrafted vs. non-handcrafted features for computer vision classification," *Pattern Recognition*, vol. 71, pp. 158–172, 2017.
- [43] R. Nijhawan, J. Das, and B. Raman, "A hybrid of deep learning and hand-crafted features based approach for snow cover mapping," *International journal of remote sensing*, vol. 40, no. 2, pp. 759–773, 2019.
- [44] P.-H. Hsu and Z.-Y. Zhuang, "Incorporating handcrafted features into deep learning for point cloud classification," *Remote Sensing*, vol. 12, no. 22, p. 3713, 2020.
- [45] C. R. Qi, H. Su, K. Mo, and L. J. Guibas, "Pointnet: Deep learning on point sets for 3d classification and segmentation," in *Proceedings of the IEEE conference on computer vision and pattern recognition*, 2017, pp. 652–660.
- [46] C. R. Qi, L. Yi, H. Su, and L. J. Guibas, "Pointnet++: Deep hierarchical feature learning on point sets in a metric space," *Advances in neural information processing systems*, vol. 30, 2017.
- [47] T. Chaton, N. Chaulet, S. Horache, and L. Landrieu, "Torch-points3d: A modular multi-task framework for reproducible deep learning on 3d point clouds," *arXiv preprint arXiv:2010.04642*, 2020.
- [48] W. Diestel, "Arbaro—tree generation for povray," 2003.
- [49] S. Fang, K. Li, J. Shao, and Z. Li, "Snunet-cd: A densely connected siamese network for change detection of vhr images," *IEEE Geoscience and Remote Sensing Letters*, vol. 19, pp. 1–5, 2021.
- [50] M.-H. Guo, J.-X. Cai, Z.-N. Liu, T.-J. Mu, R. R. Martin, and S.-M. Hu, "Pct: Point cloud transformer," *Computational Visual Media*, vol. 7, pp. 187–199, 2021.